# Thermal Induced Polymerization of L-Lysine forms Branched Particles with Blue Fluorescence

*Luigi Stagi, Luca Malfatti, Francesca Caboi, and Plinio Innocenzi\**

The polycondensation of amino acids can originate complex polymers that display fascinating structural and optical properties. Thermally induced amidation of L-lysine allows forming a branched polymer without the support of any catalyst. The polycondensation is completed at 240–250 °C; at higher temperatures, the amino acid degrades. The obtained polylysine particles have been studied by transmission electron microscopy (TEM), nuclear magnetic resonance, and infrared spectroscopy that allow for investigating the different steps of the synthesis. The resulting structure is characterized by peculiar optical properties, e.g., excitation-dependent blue fluorescence and good quantum efficiency. Hydrogen bonds and the interactions of the amino acids are considered responsible for the optical properties of both L-lysine monomer solutions at high concentrations and the branched nanopolymers.

## 1. Introduction

Polycondensation of L-lysine, an asymmetrical AB$_2$ type amino acid, can produce different types of polymeric structures [1]; polymerization through the amine in $\alpha$ or $\epsilon$ position, in particular, give $\alpha$-poly-L-lysine or $\epsilon$-poly-lysine polymers, respectively. L-lysine dendrimers,[2,3] which are perfect macromolecules with a regular and highly branched 3-dimensional structure have been also synthesized.[4] The dendrimers have been widely tested as drug and gene delivery carriers,[5] contrast agents for magnetic resonance imaging[6] bioimaging agents.[7] The L-lysine dendrimer structures are very attractive for their symmetry and regular shape, but are difficult to synthesize. Branched and hyperbranched polylysine structures represent an interesting alternative, they do not exhibit the same degree of regularity of a dendrimer but have a randomly branched structure that can be formed by simpler synthetic routes.[8]

More recently, amino acids have been also considered valuable raw materials for the synthesis of carbon dots.[9,10] Amino acids exhibit high melting point (between 200 °C and 300 °C) and furthermore, being nontoxic and common biological molecules, they are widely exploited in bioimaging and nanomedicine.[11,12] L-lysine and arginine can be produced by pyrolysis carbon dots that work well as antibacterial systems.[13] Another peculiar characteristic of lysine-derived carbon dots is the efficient fluorescence in the blue region, which makes them usable for bioimaging.[14,15] Structural investigations have clearly identified a graphitic inner core in the carbon dots,[16] but the vibrational spectroscopic measurements demonstrate the conservation of specific molecular groups, such as aminic and carboxyl groups, which add new functionalities.[14] For example, the photoluminescence appears enhanced and dependent from the excitation energy. The origin of the optical properties and the mechanisms involved in the peculiar excitation spectra are still unknown.

Inspired by the growing interest and remarkable properties of amino acid derived carbon dots, we have investigated the thermal polymerization of L-lysine in a wide range of temperatures.[17] Interestingly, nongraphitic polymeric particles with high dispersion in dimension are the resulting products (from a few hundred nanometers to a few micrometres). Furthermore, there is no evidence of aromatic moieties. The formation of L-lysine and hyperbranched polylysine has not been associated, to our knowledge, to a significant fluorescence even if the L-lysine monomer is weakly fluorescent. The branched polylysine structure exhibits instead an enhanced blue emission which is excitation-dependent in the blue region. The problem of the origin of fluorescence has been addressed by FTIR and time-resolved fluorescence spectroscopy and has been correlated with the strong interaction by hydrogen bonds of the L-lysine units, both in the branched polylysine and in the monomer at high concentration.

L. Stagi
Laboratory of Materials Science and Nanotechnology
Via Vienna 2
Department of Chemistry and Pharmacy, University of Sassari
Sassari 07100, Italy

L. Malfatti, P. Innocenzi
Laboratory of Materials Science and Nanotechnology
Viale San Pietro 43/B
CR-INSTM Department of Biomedical Sciences University of Sassari
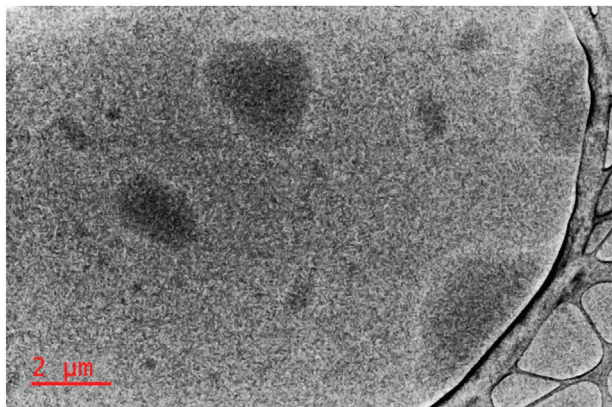Sassari 07100, Italy
E-mail: plinio@uniss.it

F. Caboi
NMR e Tecnologie Bioanalitiche
Sardegna Ricerche
Parco Scientifico e Tecnologico della Sardegna
Pula, CA 09010, Italy

ADVANCED
SCIENCE NEWS
www.advancedsciencenews.com

Macro-
molecular
Chemistry and Physics
www.mcp-journal.de

**Figure 1.** Bright-field transmission electron microscopy (TEM) image of polylysine nanoparticles.

## 2. Results and Discussion

The thermal polymerization of L-lysine,[18] which has been carried out in air starting from a powder as precursor, has allowed obtaining at the end of the purification process of polymeric nanoparticles which have been characterized using a combination of different techniques to identify their structures.

Transmission electron microscopy (TEM) images of polylysine nanoparticles (**Figure 1**) show the formation of spherical-like structures with a broad distribution in size. The estimated size is in the range between 800 nm and 3.5 $\mu$m. However, a precise measure of the diameter is difficult because of the low electronic contrast. The particles are amorphous and do not show any evidence of crystalline organization, which supports the formation of interconnected polymeric structures with a low degree of densification (Figure S1, Supporting Information).
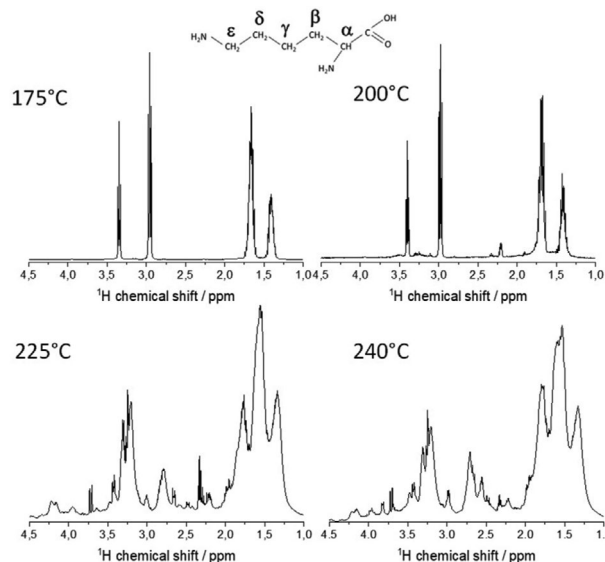
The effect of the thermal treatment has been studied by in situ FTIR spectroscopy to detect the structural changes as a function of the temperature. **Figure 2**a shows the temperature ($y$ axis) – wavenumber ($x$ axis) – intensity (absorbance false color scale) infrared graph in the range 1825–1475 cm$^{-1}$ range. The thermal treatment has been performed in air from 25 up to 240 °C.

Figure 2b shows the reference spectra of L-lysine (black line) at 25 °C (powder sample) and after thermal treatment at 240 °C (red line) in the range 1800–1250 cm$^{-1}$ wavenumber region. In this interval, the spectrum of L-lysine shows the characteristic bands of $C_\beta$ twisting (1323 cm$^{-1}$), $C_\beta$ wagging (1353 cm$^{-1}$), $-COO^-$ antisymmetric stretching, CH$_2$ deformation (1442 and 1454 cm$^{-1}$), N−H bending, and $-COO^-$ symmetric stretching.[19] The spectrum after thermal treatment at 240 °C shows the typical band of amide I, C=O stretching, at 1668 cm$^{-1}$ while the $-COO^-$ bands clearly disappear indicating the completion of the amidation reaction with polycondensation of L-lysine. The amidation reaction is observed to begin around 225 °C (**Figure 3**).
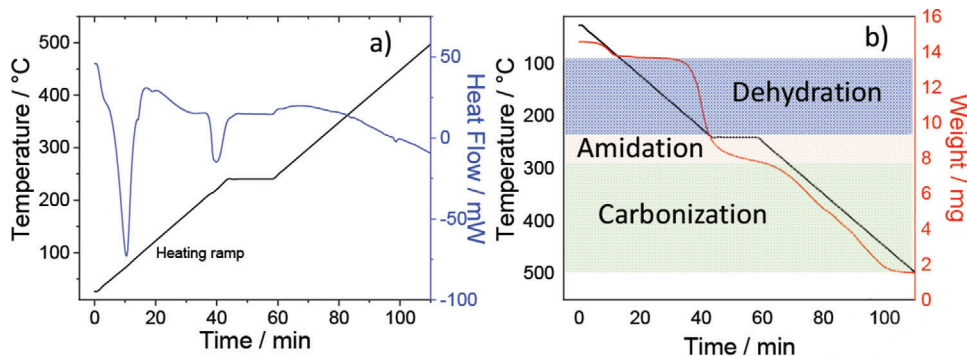
The thermal polymerization of L-lysine can form different polycondensed structures, from branched to linear. The linear forms are poly($\epsilon$-lysine), and a poly($\alpha$-lysine), which are formed upon linking with the $\epsilon$-amino group ($\epsilon$ linear, $L_\epsilon$) or the $\alpha$-amine group ($\alpha$-linear, $L_\alpha$). $^1$H NMR spectra of L-lysine are characterized by the chemical shifts at 3.74 ($H_\alpha$), 3.02 ($H_\epsilon$), 1.89 ($H_\beta$), 1.71 ($H_\delta$), and 1.46 ($H_\delta$) ppm. As the polycondensation reactions proceed
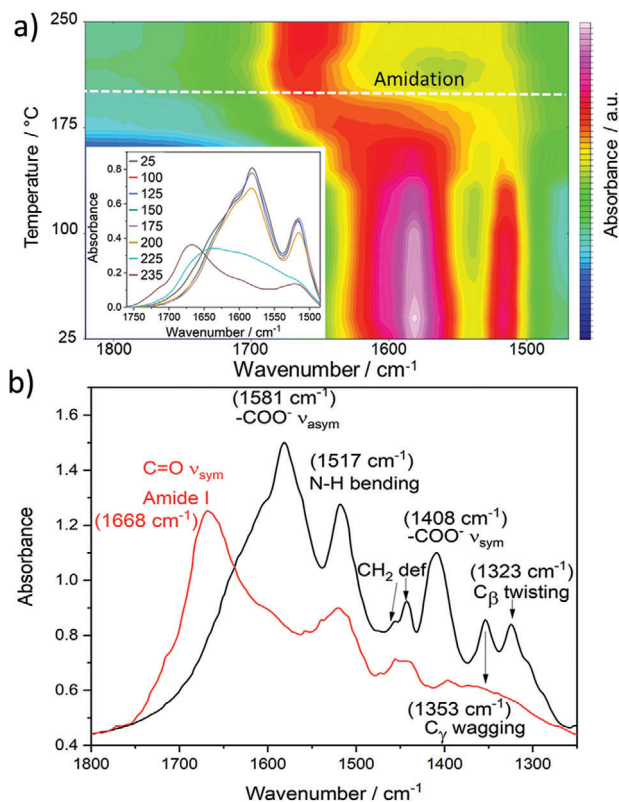


**Figure 2.** a) Temperature-wavenumber-intensity infrared graph obtained by in situ Fourier-transform infrared (FTIR) absorption spectra in the 1825–1475 cm$^{-1}$ range during thermal treatment in air of L-lysine from 25 to 250 °C. The absorbance is shown in a false color scale. b) Fourier-transform infrared (FTIR) absorption spectra in the 1800–1250 cm$^{-1}$ interval. The reference spectra of L-lysine (black line) at 25 °C (powder sample) and after thermal treatment at 240 °C (red line) are shown.



**Figure 3.** $^1$H NMR spectra of thermally treated L-lysine at different temperatures.

ADVANCED
SCIENCE NEWS
www.advancedsciencenews.com

acro-
olecular
Chemistry and Physics
www.mcp-journal.de

**Figure 4.** a) DTA analysis of the L-lysine from 25 °C to 500 °C (blue line). The black line shows the thermal ramp with a 20 min dwell at 250 °C. b) TGA analysis of the L-lysine from 25 °C to 500 °C (blue line). The black line shows the thermal ramp with a 20 min dwell at 250 °C.

from 225 °C new signals are detected, which are correlated with the formation of highly branched polymeric structure. In particular, the chemical shifts at 4.14 ppm ($\alpha$-CH protons in dendritic units), 3.42 ppm (terminal $\alpha$-CH protons), 3.31 ppm (terminal $\alpha$-CH protons), 3.24 ppm ($\epsilon$-linear units, $L_\epsilon$)), 3.19 ppm ($\epsilon$-CH$_2$ close to an amide bond, dendritic and $\epsilon$ -linear), 2.7 ppm ($\epsilon$-CH$_2$ group, close to the amino group in $\alpha$-linear and terminal structural units) indicate the formation of a dendron-like structure.[20] The $^1$H NMR spectra at 240 °C show also that some unreacted L-lysine is also present, while linear polymeric structures are also formed, in particular, poly($\epsilon$-lysine), with the characteristic chemical shifts at 3.29 and 3.19 ppm, and poly($\alpha$-lysine), chemical shifts at 3.95 and 2.67 ppm. Furthermore, the line broadening well supports the formation of a hyperbranched polymer structure. The final structure of the nanopolymers, obtained via thermal polycondensation, is therefore formed by a highly branched polymer which should be interconnected with a small fraction of poly($\epsilon$-lysine) and poly($\alpha$-lysine).[21]
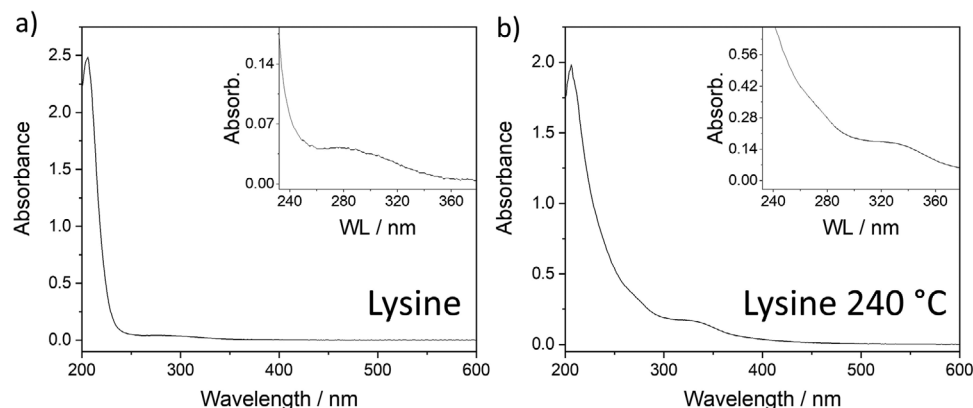
The DTA curve (**Figure 4**a) is characterized by two endothermic events, one peaking at 90 °C and assigned to dehydration of L-lysine and a second one peaking at 225 °C which is attributed to the amidation reactions. At temperatures higher than 350 °C carbonization of the samples is observed. The weight loss also highlights the three thermal events (Figure 4b). In the first stage of dehydration the sample loses 37% of his weight due to thermal dehydration of absorbed water, in the second step the L-lysine polycondenses via amidation reactions with release of water molecules and a further 7% weight decrease. Finally at temperatures, from 350 °C the sample carbonizes and loses further weight.

These data are in good accordance with FTIR and NMR experimental findings. The formation of polylysine, which is achieved without the support of any catalyst, is observed as a consequence of the amidation reaction. The effects of thermal-induced polymerization on the optical properties of L-lysine have been investigated by optical absorption and fluorescence measurements. The full comprehension of amino acid interactions and their optical features in aqueous solutions is still unclear. Nonaromatic amino acids are expected to display a strong absorption in the far UV region (200–250 nm), and the corresponding fluorescence should be absent or very weak. The hypothesized scarce emission is in evident contrast with several experimental findings which show, instead, a significant fluorescence and structured absorbance for

several amino acids.[22–24] These experimental results make arduous to explain the UV-Vis and photoluminescence spectra of various amino acids, particularly at high concentrations and in peptide systems.[25] Taking this into account, the optical properties of L-lysine and its derived branched polymeric structure obtained via thermal amidation reactions have been investigated in detail. **Figure 5** shows the UV-Vis absorption of L-lysine (Figure 5a) and branched poly-lysine (Figure 5b) in water. A strong absorption band, extended from around 205 to 250 nm, characterizes the L-lysine UV-Vis spectrum. The inset in Figure 5a shows the detail of a weak band at 270–280 nm extending up to 360 nm. After thermal condensation, the main absorption band widens toward higher wavelengths, and the features between 240 and 360 nm acquire a more complex structure (Figure 5b). This absorption region (inset in Figure 5b) reveals the presence of two bands. The band at around 277–280 nm might results from the full width at half maximum (FWHM) increase of the 205 nm absorption band or the enhancement of the low energy band observed in the monomer. The band at 340 nm is a new contribution that stemmed from the polymerization process. The overall effect of the L-lysine thermal-induced polymerization on the optical properties is the extension of the absorbance in the visible range with a long tail up to around 500 nm.

It has been reported that the L-lysine does not display any absorption in the near UV region at low concentrations. However, the experiments performed using L-lysine monochloride on a wide interval of concentrations in buffered solutions at pH 7 have shown that the absorption band at 277 nm can be due to the interaction between different molecules rather than intramolecular electronic transitions.[26] Therefore, monitoring the L-lysine absorption at 270 nm is a reliable method to study the aggregation states in proteins that include lysine units.[27] The experimental observations have revealed the tendency of L-lysine to aggregate in aqueous solutions by the strong interaction of side chains.[24] A strong noncovalent interaction has also been observed in other nonaromatic amino acids in the solid form, such as L-histidine and L-glutamine,[26] and to less extent in glycine and L-alanine.[28]

After polymerization, the optical absorption undergoes a pronounced modification that accounts for the formation of new covalent bonds and arguably a stronger hydrogen bond interaction with the decrease of molecular mutual distances (vide infra). Amide groups (−(C=O)N) generally absorb in the

ADVANCED
SCIENCE NEWS
www.advancedsciencenews.com

[M] acro-molecular
Chemistry and Physics
www.mcp-journal.de

**Figure 5.** Optical absorption (UV-Vis) spectra of a) L-lysine (0.01 M) and b) L-lysine after thermal treatment at 240 °C (1 g L⁻¹). The insets in the graphs show the low intensity absorption bands in the region between 235 and 370 nm.

far UV region (<200 nm) with a possible redshift in a strong polar solvent.[29,30] In the light of this, the new band between 320 and 360 nm is barely explainable by the formation of the amide groups after dehydration and polymerization of L-lysine units. Similar absorption features are identifiable in the polymeric condensation of citric acid and amino rich molecules, such as tris(hydroxymethyl)aminomethane (Tris)[31] or ethylenediamine (EDA).[32] In these works, the polymeric structure is supported by the formation of amino groups units. The corresponding optical properties have been examined by quantum mechanical calculations but failed in reproducing the experimental results. In addition, the increase of the modelled cluster extension does not significantly improve the simulations. A similar discrepancy can also be encountered in monomeric proteins. For example, the absorbance of the protein $\alpha_3$C in the near UV and visible has been theoretically reproduced by simulating the photoinduced charge transfer mechanism among sidechains of different amino acids.[33] These findings indicate the importance of the intermolecular interaction by close amino acids in the interpretation of peptides optical spectra in the visible range. In our case, the enhancement of UV-Vis absorption in the near UV region can be attributed to a strong interaction by neighboring L-lysine units held together by amide bonds. Therefore, we have studied the steady-state and time-resolved luminescent properties of the L-lysine monomer and the effect of forming a branched polylysine structure after thermal treatment.

**Figure 6** shows the fluorescence response of L-lysine and branched polylysine in the 300-600 nm range by a 3D plot. The highly asymmetric intensity pattern reveals a marked excitation dependence in the L-lysine monomer. Although the intensity maximum is at 415 nm under excitation at 330 nm (QY = 1.9%), we still observe a not negligible fluorescence at 450 nm by exciting at 350 nm. The concentration of 0.1 M falls in the range of luminescence intensity linearity, and the concentration and aggregation-induced quenching in this range is not expected. Nevertheless, the excitation-dependent fluorescence a dispersion of absorbing species, and the corresponding excitation-dependent fluorescence can result from the hydrogen bonds that promote the interaction among monomers and the aggregates. After thermal treatment, the polymeric L-lysine

displays a significant shift of the fluorescence up to 460 nm. The dependence on the excitation accounts for the multiplicity of optical centres in the polymeric matrix. Differently from L-lysine monomer solutions, the vibrational and rotational motions in the polymeric structure decrease, allowing for a stronger interaction between the L-lysine units. The reduced molecular mobility affects the efficiency of the blue emission that exhibits a quantum yield of 7.4%, in perfect accordance with the reported values for recrystallized L-lysine.[9]

The dynamics of carrier recombination complies with the trend observed by steady-state measurements. **Figure 7** shows the fluorescence decay profile under excitation at 340 nm. Both luminescence profiles decay through a double-exponential law:
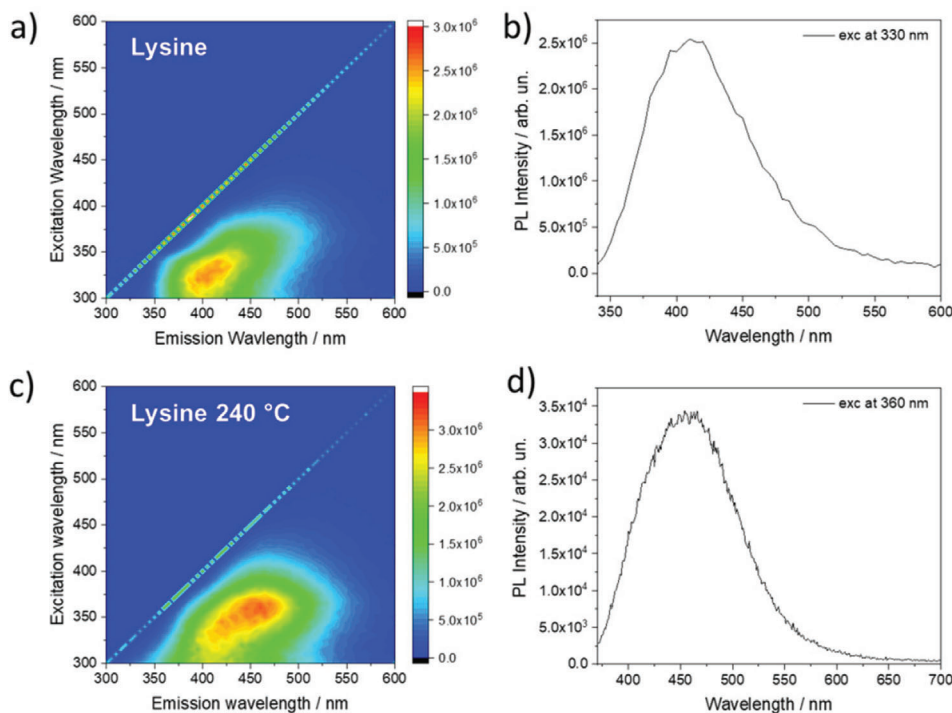
$$I = I_1 \exp(-t/\tau_1) + I_2 \exp(-t/\tau_2) \tag{1}$$

The average lifetime, $\tau^*$, is defined as[34]:

$$\tau^* = \frac{I_1 \tau_1^2 + I_2 \tau_2^2}{I_1 \tau_2 + I_2 \tau_2} \tag{2}$$

The average lifetime of L-lysine in aqueous solution is 4.2 ns, while the polymeric L-lysine decays with a lifetime of 10.6 ns. This considerable difference is attributed to the polymeric structure, which inhibits nonradiative recombination in the more rigid structure where vibration and rotational motions are partially hindered.

The optical properties of polylysine suggest that the formation of H-bonding should be at least partially responsible of the differences with L-lysine. The presence of hydrogen bond can be probed by infrared absorbance spectra. The higher wavenumber region of the L-lysine FTIR spectra, 3750–2250 cm⁻¹, is characterized by several overlapping absorption bands, whose attribution has not yet been clarified (**Figure 8**).

The more intense and sharper absorption bands at 2938 and 2861 cm⁻¹ are unambiguously assigned to $CH_2$ $\nu_{asym}$ and $CH_2$ $\nu_{sym}$, respectively. The L-lysine molecules can assume many different conformations and theoretical calculations have allowed to identify four types of possible backbones.[35] These different conformations are stabilized by intramolecular H-bonding, such as OH···N, $NH_2$···O=C or $NH_2$···OH. H-bonding plays,

ADVANCED
SCIENCE NEWS
www.advancedsciencenews.com

Macro-
molecular
Chemistry and Physics
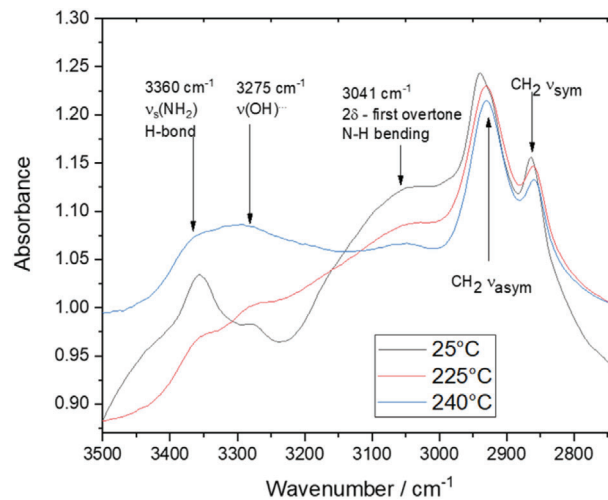www.mcp-journal.de

**Figure 6.** Excitation (*y*)-emission (*x*)-intensity (*z*) plot and photoluminescence spectra of 0.1 M L-lysine (a,b) and branched L-lysine (c,d).
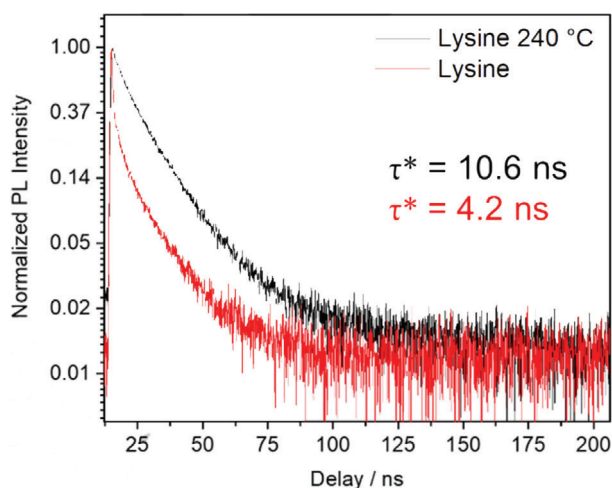


**Figure 7.** Time-resolved fluorescence of under excitation at 340 nm. The fluorescence is monitored at 415 nm in L-lysine and 460 nm in branched polylysine.



**Figure 8.** Fourier-transform infrared (FTIR) absorption spectra in the 3500–2730 cm$^{-1}$ interval of reference L-lysine (black line) at 25 °C (powder sample) and after thermal treatment at 225 (blue line) and 240 °C (red line).

therefore, a fundamental role in L-lysine derived structures, such as poly(α)lysine or poly(ε)lysine polymers and branched polylysine.[36]

In the 3750 – 2250 cm$^{-1}$ region, besides the CH$_2$ stretching modes, three other overlapped bands are detected at 3360, 3275, and 3041 cm$^{-1}$. They have been tentatively assigned to stretching of NH$_2$ (3360 cm$^{-1}$), stretching of H-bonded OH (3275 cm$^{-1}$), and the first overtone of NH bending also involved in H bonding (3041 cm$^{-1}$). As it is involved in the reaction, the NH$_2$ stretching

band at 3360 cm$^{-1}$ decreases in intensity as the reaction proceeds. There is very good correspondence of the NH$_2$ stretching band with DTA and NMR data, and at 225 °C a strong decrease in intensity is observed in correspondence to the amidation and polymerization of L-lysine. At the same time, an increase in intensity of the absorption bands at 3275 and 3041 cm$^{-1}$, which are assigned to H-bonding, is observed. On the other hand, NH$_2$ groups do not disappear completely and an overlapping band,

still assigned to this mode, is observed in samples treated at higher temperature, and may also be involved in H-bonding. The branched structure of the polylysine nanopolymers favors the formation of H-bonds which are supposed to play an important role in stabilizing the structure and in affecting the optical response.

## 3. Conclusions

Thermal-induced polymerization of L-lysine monomers occurs through the formation of amide bonds producing a complex branched structure. Branched polylysine forms between 225 °C and 240 °C by an amidation process which is thermally activated from around 225 °C. At higher temperatures, the polymer undergoes a carbonization process that likely promotes the formation of graphitic structures. Monomers and polymers are soluble in aqueous solutions, and both show relevant visible blue emission. In particular, the blue fluorescence of polylysine, which is not merely explainable by the presence of amide groups, increases in intensity and redshifts in comparison with the L-lysine monomers. As suggested by steady-state spectroscopy measurements, L-lysine and poly-L-lysine tend to aggregate, resulting in an excitation dependent fluorescence pattern. Furthermore, time-resolved measurements and increased quantum yield indicate that the polymeric network inhibits the effect of nonradiative recombinations induced by molecular motions. The optical and vibrational analyses indicate that weak hydrogen bonds represent a crucial parameter by fostering the intermolecular interaction and adding peculiar fluorescent properties to amino acid based polymers to create fluorophores by a simple thermal-induced polymerization.

## 4. Experimental Section

Branched polylysine nanoparticles have been synthesized by thermal polymerization. Commercial L-lysine ((S)-2,6-Diaminocaproic acid) powder (Sigma-Aldrich, crystallized, ≥98.0% (NT), $H_2N(CH_2)_4CH(NH_2)CO_2H$, has been placed in a ceramic crucible and heated up to 240 °C for 5 h and let it cool down to 20 °C before any further treatment. After the thermal treatment, the obtained brown-black solid has been dispersed in milli-Q water, sonicated for 15 min and then centrifugated at 9000 rpm for 20 min. The supernatant has been collected and dialyzed against water for 24 h with a dialysis tube (benzoylated, avg. flat width 32 mm (1.27 in.)), replacing the water every 12 h. Then, the resulting nanomaterials have been freeze-dried for 24 h and kept at 4 °C before characterization.

TEM bright-field images were obtained by using a FEI TECNAI 200 operating at 200 kV with field emission electron guns. Before analysis, the material was dispersed in ethanol and ultrasonicated for 10 min. Afterward, the solutions containing the nanoparticles were cast on grids made by Cu and covered with an ultrathin layer of carbon (nominally of 3 nm) mounted on a lacey carbon film. After drying at room temperature, the grids were directly used for the measures. The particle size was estimated by measuring at least ten different particles on 5 images taken from different areas of the grid.

Attenuated total reflectance-Fourier-transform infrared (ATR-FTIR) analysis was carried out by an ATR accessory coupled with an infrared Vertex 70 interferometer (Bruker). The ATR spectra were recorded in the range 4000–400 cm$^{-1}$ with a 4 cm$^{-1}$ resolution.

In situ Fourier-transform infrared spectra on sample powders in potassium bromide (KBr, IR 99%, Sigma) were collected in an electrical heating jacket in transmission geometry (Specac).

UV-Vis absorption spectra were collected by a Nicolet Evolution 300 UV-Vis spectrophotometer (Thermo Fisher) with a bandwidth of 1.5 nm.

Fluorescence spectroscopy measurements were performed using a Horiba Jovin Yvon Fluoromax-3. Typically, 3D PL maps of aqueous solutions were recorded from 200 to 600 nm. Photoluminescence quantum yield (QY) measurements have been performed using the quanta-$\varphi$ (HORIBA) integrating sphere accessory, attached to the "NanoLog" Horiba Jobin Yvon spectrofluorometer.

X-ray diffraction (XRD) patterns were collected using a SmartLab X-ray powder diffractometer (Rigaku, Tokyo, Japan) in Bragg–Brentano geometry with Cu Kα radiation ($\lambda = 1.54178$ Å) and a graphite monochromator in the diffracted beam.

$^1$H-NMR spectra were recorded at 25 °C on a Bruker Avance III 400 MHz spectrometer. Deuterium Oxide ($D_2O$) + Tetramethylsilane (TMS, 0.05% v/v) was used as the solvent. Deuterium oxide 99.9 atom% D, containing 0.05 wt% 3-(trimethylsilyl)propionic-2,2,3,3-d4 acid sodium salt was purchased from Sigma–Aldrich. Samples were dissolved in 0.6 mL $D_2O$ and transferred to 5 mm NMR sample tube. TMS, used as internal standard, was calibrated as $\delta = 0.00$ ppm. The experimental parameters were: 1H NMR: Pulse angle of 90°, acquisition time of 2.5 s, 512 repetitions, and spectral width of 12 ppm.

## Supporting Information

Supporting Information is available from the Wiley Online Library or from the author.

## Conflict of Interest

The authors declare no conflict of interest.

## Data Availability Statement

Research data are not shared.

[1] S. Chen, S. Huang, Y. Li, C. Zhou, *Front. Chem.* **2021**, *9*, 169.

[2] N. Hegde, V. Velingkar, B. Prabhakar, *Int. J. Pept. Res. Ther.* **2019**, *25*, 1539

[3] B. J. Boyd, L. M. Kaminskas, P. Karellas, G. Krippner, R. Lessene, C. J. H. Porter, *Mol. Pharm.* **2006**, *3*, 614

[4] M. Thompson, C. Scholz, *Nanomaterials* **2021**, *11*, 1119.

[5] M. Gorzkiewicz, M. Konopka, A. Janaszewska, I. I. Tarasenko, N. N. Sheveleva, A. Gajek, I. M. Neelov, B. Klajnert-Maculewicz, *Bioorg. Chem.* **2020**, *95*, 103504.

[6] G. Zu, M. Liu, K. Zhang, S. Hong, J. Dong, Y. Cao, B. Jiang, L. Luo, R. Pei, *Biomacromolecules* **2016**, *17*, 2302

[7] N. A. Patil, B. Kandasubramanian, *Eur. Polym. J.* **2021**, *146*, 110248.

[8] J.-P. Francoia, L. Vial, *Chem. - Eur. J.* **2018**, *24*, 2806

[9] S. Sarkar, K. Das, M. Ghosh, P. K. Das, *RSC Adv.* **2015**, *5*, 65913

[10] J. Jiang, Y. He, S. Li, H. Cui, *Chem. Commun.* **2012**, *48*, 9634

[11] N. Sahiner, S. S. Suner, M. Sahiner, C. Silan, *J. Fluoresc.* **2019**, *29*, 1191

[12] S. Pandit, P. Behera, J. Sahoo, M. De, *ACS Appl. Bio Mater.* **2019**, *2*, 3393

[13] P. Li, F. Han, W. Cao, G. Zhang, J. Li, J. Zhou, X. Gong, G. Turnbull, W. Shu, L. Xia, B. Fang, X. Xing, B. Li, *Appl. Mater. Today* **2020**, *19*, 100601.

[14] H. V. Xu, X. T. Zheng, Y. Zhao, Y. N. Tan, *ACS Appl. Mater. Interfaces* **2018**, *10*, 19881

[15] X. Tang, H. Yu, B. Bui, L. Wang, C. Xing, S. Wang, M. Chen, Z. Hu, W. Chen, *Bioact. Mater.* **2021**, *6*, 1541

[16] J. Ren, L. Stagi, P. Innocenzi, *Prog. Solid State Chem.* **2021**, *62*, 100295.

[17] K. Harada, *Bull. Chem. Soc. Jpn.* **1959**, *32*, 1007

[18] M. R. Heinrich, D. L. Rohlfing, E. Bugna, *Arch. Biochem. Biophys.* **1969**, *130*, 441

[19] B. Hernández, F. Pflüger, N. Derbel, J. De Coninck, M. Ghomi, *J. Phys. Chem. B* **2010**, *114*, 1077

[20] M. Scholl, T. Q. Nguyen, B. Bruchmann, H.-A. Klok, *Macromolecules* **2007**, *40*, 5726

[21] Y.-Z. Wang, X.-X. Deng, L. Li, Z.-L. Li, F.-S. Du, Z.-C. Li, *Polym. Chem.* **2013**, *4*, 444

[22] I. Mandal, S. Manna, R. Venkatramani, *J. Phys. Chem. B* **2019**, *123*, 10967

[23] R. Ravanfar, C. J. Bayles, A. Abbaspourrad, *Cryst. Growth Des.* **2020**, *20*, 1673

[24] X. Chen, W. Luo, H. Ma, Q. Peng, W. Z. Yuan, Y. Zhang, *Sci. China Chem.* **2018**, *61*, 351

[25] A. D. Stephens, M. N. Qaisrani, M. T. Ruggiero, G. Díaz Mirón, U. N. Morzan, M. C. González Lebrero, S. T. E. Jones, E. Poli, A. D. Bond, P. J. Woodhams, E. M. Kleist, L. Grisanti, R. Gebauer, J. A. Zeitler, D. Credgington, A. Hassanali, G. S. Kaminski Schierle, *Proc. Natl. Acad. Sci.* **2021**, *118*, e2020389118.

[26] L. Homchaudhuri, R. Swaminathan, *Chem. Lett.* **2001**, *30*, 844

[27] L. Homchaudhuri, R. Swaminathan, *Bull. Chem. Soc. Jpn.* **2004**, *77*, 765

[28] B. Z. Chowdhry, T. J. Dines, S. Jabeen, R. Withnall, *J. Phys. Chem. A* **2008**, *112*, 10333

[29] A. R. Goldfarb, L. J. Saidel, E. Mosovich, *J. Biol. Chem.* **1951**, *193*, 397

[30] E. B. Nielsen, J. A. Schellman, *J. Phys. Chem.* **1967**, *71*, 2297

[31] R. Ludmerczki, L. Malfatti, L. Stagi, M. Meloni, C. M. Carbonaro, M. F. Casula, D. Bogdán, S. Mura, I. M. Mándity, P. Innocenzi, *Chem. - Eur. J.* **2021**, *27*, 2543

[32] L. Vallan, E. P. Urriolabeitia, F. Ruipérez, J. M. Matxain, R. Canton-Vitoria, N. Tagmatarchis, A. M. Benito, W. K. Maser, *J. Am. Chem. Soc.* **2018**, *40*, 12862

[33] S. Prasad, I. Mandal, S. Singh, A. Paul, B. Mandal, R. Venkatramani, R. Swaminathan, *Chem. Sci.* **2017**, *8*, 5416

[34] L. Stagi, S. Mura, L. Malfatti, C. M. Carbonaro, P. C. Ricci, S. Porcu, F. Secci, P. Innocenzi, *ACS Omega* **2020**, *5*, 10958

[35] B. Boeckx, G. Maes, *J. Phys. Chem. B* **2012**, *116*, 12441

[36] M. Rozenberg, G. Shoham, *Biophys. Chem.* **2007**, *125*, 166